Magnetized Target Fusion in a Spheroidal Geometry With Standoff Drivers

Y. C. F. Thio, NASA Marshall Space Flight Center,
E. Panarella, Advanced Laser & Fusion Technology, Ottawa, Canada,
R. C. Kirkpatrick, C. E. Knapp, F. Wysocki, Los Alamos National Laboratory,
P. Parks, General Atomic, Inc., San Diego, California,
G. Schmidt, NASA Marshall Space Flight Center, Huntsville, Alabama.

Abstract

An embodiment of magnetized target fusion (MTF) with the potential that the drivers can be positioned in a standoff distance from the site of the fusion burn is proposed. The magnetized target plasma is formed out of two merging compact toroids, and is imploded by a spherical plasma liner formed out of the merging of a number (nominally 60) of high momentum density plasma jets. These plasma jets are produced by highly efficient electromagnetic accelerators. They also carry the main fusion fuel. The implosion dynamics is studied in three phases: the preliminary shock heating and compression, the acoustic compression, and the containment of the burning target and liner. Mathematical models are developed to model these three phases of the implosion dynamics, and have been implemented in a suite of computer codes. Preliminary results produced by the models have been very encouraging, showing the great potential of the proposed MTF scheme. The scheme has a low energy threshold for economic breakeven, and has the potential of high wall-plug energy gain of more than 50 or so. Moreover, the pulsed power drivers are very modest and can be accommodated with current state of the art and existing facilities. The embodiment thus potentially provides a low-cost and fast R&D path towards demonstrating practical fusion energy and followed-on commercialization.

1. Introduction

In magnetized target fusion (MTF), an imploding material liner is used to compress a magnetized plasma to fusion condition and to confine the resulting burning plasma inertially to obtain the necessary energy gain. By choosing a physics and engineering regime intermediate between the two extremes of conventional magnetic confinement fusion (MFE) and inertia confinement fusion (ICF), MTF seeks to avoid the physics and engineering problems of these two conventional approaches to fusion.

Specifically, the density regime and time scale of MTF is intermediate between MFE and ICF. This regime is important for three reasons. (1) Fusion reactivity scales as density squared, which is increased by many orders of magnitude over conventional MFE. (2) All characteristic plasma scale-lengths decrease with density. Hence, system size is naturally reduced at high density. (3) The presence of the magnetic field in the target plasma greatly slows down the thermal conduction losses to the material liner, thus allowing relatively slow compression to be used with liner produced by highly efficient electromagnetic drivers. It reduces the required power and precision to compress and heat plasma to fusion-relevant conditions compared with ICF, and brings the pulsed-power requirements within reach of current state of the art. For these reasons, MTF promises to be a low-cost approach to fusion[1,2,3].

Solid liners have been proposed for compressing the target for MTF, especially for a near-term demonstration of the scientific principles of MTF. One frequent criticism of solid-liner driven MTF relates to its reactor potential. Though reactor scenarios have been proposed for solid-liner driven MTF, critics of MTF have pointed out three potential practical difficulties with solid-liner driven MTF. Firstly, the drivers for imploding the liner need to have sufficient stand-off distance from the point of the fusion combustion for the hardware to be re-usable, and this might be difficult to achieve in the case of solid liners. Secondly, the cost of manufacturing the solid liner tends to drive the economic breakeven energy level into the multi-gigajoule range, thus increasing the initial capital cost of the power plant. Thirdly, the solid debris from the liner might present a problem to the first wall of the reactor.

This paper is a response to these criticisms of MTF, by proposing an embodiment of MTF that will avoid all these difficulties. In the proposed embodiment, a gaseous (plasma) liner is used instead, and is formed in a standoff manner. It has a low energy threshold for economic breakeven, and has the potential of high wall-plug energy gain of more than 50 or so. Moreover, the pulsed power drivers are very modest and can be accommodated with current state of the art and existing facilities. The embodiment thus potentially provides a low-cost and fast R&D path towards demonstrating practical fusion energy and followed-on commercialization.

---

[1] I. R. Lindemuth and R. C. Kirkpatrick, "The promise of magnetized fuel: High gain in inertia confinement fusion," *Fusion Technology*, Vol. 20, pp. 829 – 833, 1991.

[2] R. C. Kirkpatrick and I. R. Lindemuth, "Magnetized Target Fusion, An Overview of the Concept," *Current Trends in International Fusion Research*, ed. E. Panarella, Plenum Press, New York, 1997.

[3] R. Siemon, et al. A Proposal for aProof-of-Principles Experiment for Magnetized Target Fusion. Paper presented at the American Physical Society Division of Plasma Physics Meeting, Nov 16 – 20, 1998, New Orleans, LA.

2. The Proposed Approach

Figure 2.1 illustrates the scheme. Two compact toroids containing fusionable materials are introduced into a spherical reactor vessel (typically about 2 m or more in radius) in a diametrically opposing manner[4,5] Embedded in the compact toroids are magnetic fields in force-free Woltjer-Wells-Taylor's state of minimum energy[6] which are known experimentally to be extraordinarily stable. They collide in the center to form an initial magnetized plasma. A spherical distribution of plasma jets are then launched from the periphery of the vessel, coalescing to form a spherically converging plasma liner. On impact with the central plasma, the plasma liner sends a shock wave through it, shock heating it to some elevated temperature (above a few hundreds eV). The high temperature immediately raises the electrical conductivity of the plasma to the extent that it traps the magnetic flux inside the central plasma. Because of the dominant radial momentum density of the plasma liner, it continues to implode towards the center. The target plasma is further compressed by the plasma liner and heated near-adiabatically to conditions for thermonuclear burn, the magnetic flux being compressed with it, raising the magnetic fields towards megagauss levels. The compression is near adiabatic for two reasons: (1) the presence of the megagauss magnetic field strongly inhibits electron thermal conduction losses by several orders of magnitude, (2) the plasma density of the central plasma is kept relatively low so that bremsstrahlung losses are small. Synchrotron radiation losses can also be shown to be negligible. The thermal loss rates are sufficiently low that the compression heating can be achieved relatively slowly using plasma jets with velocity of the order of 10 - 100 cm per microsecond. These plasma jets can be produced using Lorentz force coaxial plasma guns as shown in Figure 2.2. The possibility of forming a plasma liner out of the merging of plasma jets has been demonstrated experimentally by Degnan using a cylindrical array of plasma guns[7].

The plasma liner is a composite structure consisting of two layers, an inner layer carrying the main fusion fuel, and an outer tamping layer carrying a heavy gas such as argon. This composite structure can be formed either as part of the process of refueling the plasma guns, or by a properly synchronized launch of two sets of spherically distributed plasma jets, each set carrying the required gas. The radial convergence of the plasma liner is halted abruptly by the nuclear burning central plasma sending a stagnating shock expanding outwards through the plasma liner, compressing the plasma liner to form a highly dense cold fuel layer on the inside. The cold fuel layer is ignited by the nuclear burning central plasma serving therefore as a "hot spot". The pressure and the inertia of the shocked and compressed liner provide the inertia confinement for itself and the nuclear burning hot spot. When the expanding shock wave reaches the outer boundary of the plasma liner, the liner expands and a rarefaction wave emanates radially inwards

[4] D.R. Wells, P.E. Ziajka, and J. L. Tunstall, "Hydrodynamic confinement of thermonuclear plasmas (Plasma liner confinement)," *Fusion Technology*, vol. 9, p. 83 – 95 (1986).
[5] J.H. Degnan, "Compact toroid formation, compression, and acceleration," Phys. Fluids B, vol 5(8), p. 2938 – 2958 (1993)
[6] J.B. Taylor, Phys. Rev. Lett, **33**, p. 1139 (1974).
[7] J.H. Degnan, W.L. Baker, M. Cowan, J.D. Graham, J.L. Holmes, E.A. Lopez, D.W. Price, D. Ralph, and N.F, Roderick, "Operation of cylindrical array of plasma guns."

Figure 2.1 Magnetized Target Fusion with an Imploding Plasma Liner

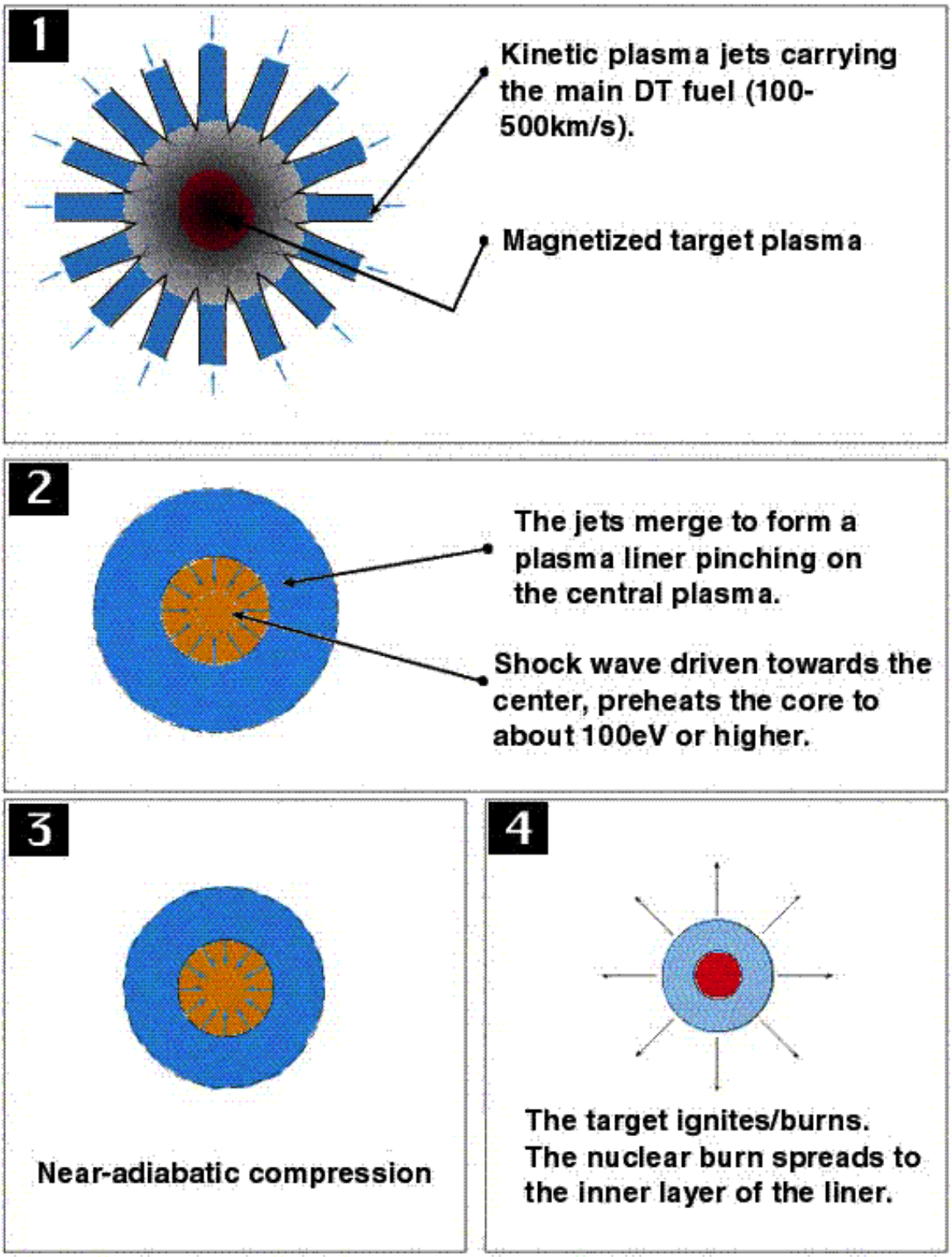

from the surface of this outer boundary. This results in the expansion and the disassembly of the plasma liner, terminating the confinement of the nuclear burning fireball. The fusion confinement time is approximately the sum of the transit time of the stagnating shock and twice the transit time of the rarefaction wave through the cold fuel layer. If the cold fuel layer is sufficiently thick and dense to trap and re-deposit a fraction of the energy of the charged particles from the fusion reactions, it is possible for a fusion burn wave to spread through the cold fuel, and thus multiplying the energy gain of the hot spot. Excessively high gain is not required here as plasma accelerators are relatively efficient.

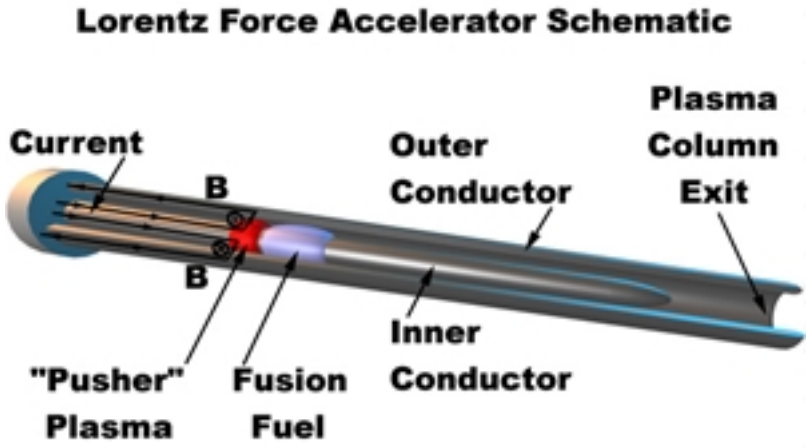

Figure 2.2 Coaxial plasma guns for producing the high velocity plasma jets

The conditions of the plasma liner and the target plasma at the instant of impact (engagement) determines the subsequent dynamics of implosion. Typical parameters for the plasma liner at this instant of impact are: velocity – 125 km/s, particle density – 10^{20} cm^{-3}, total energy – 10 MJ. Typical parameters for the target plasma at the instant of impact are: density – 10^{18} cm^{-3}, temperature – 2 eV, magnetic field – 1 T. Typical parameters for the target plasma at peak compression to produce gainful fusion burn are: temperature – 10 keV, density – 10^{21} cm^{-3}, pressure – 30 Mbar, radius – 2.5 mm, confinement time – 0.05 μs.

The concept is an evolution from a combination of previously studied concepts including impact fusion[8], compression of compact toroids[9], theta and spherical pinches[10], and electromagnetic accelerators[11].

[8] Proceedings of the Workshop in Impact Fusion, ed. F. Ribe, Los Alamos National Laboratory, Los Alamos, NM, 1978.
[9] D.R. Wells, et al (1986) ; C.W. Hartman and J.H. Hammer, "New type of collective acceleration," Phys. Rev. Lett., 48: 929 – 932, April, 1982.
[10] E. Panarella, "The spherical pinch," *J. Fusion Energy*, **6**, p. 285 (1987).
[11] Y. C. Thio, et al. "Feasibility Study of Railgun as a Driver for Impact Fusion, Final Report," Report DoE/ER/13048-3, Contract DE-AC02-83ER13048, U.S. Department of Energy, Germantown, Washington, D.C., June 1986.

3. The Contact Surface and Flux Trapping

A few fundamental questions about scheme need to be addressed at the outset: (1) Would a contact surface be formed between the plasma liner and the target plasma to provide a "piston head" in imploding the target plasma, or would the interpenetration of plasmas prevent such a contact surface from being formed? (2) Would the magnetic flux be trapped in the target plasma and be compressed by the liner?

The thickness of the contact surface is of the order of the collision length scales of the particles in the liner. The collision length (mean free path) between the same species of particles in a plasma is given by[12],

$$\lambda = \frac{25\pi\varepsilon_0^2 (kT)^2}{Z^4 ne^4 \ln\Lambda}$$

As we shall later, the shocked temperature of the liner initially is about 100 eV. With a density of the order of 10^{20} cm^{-3}, the collision length can be estimated at about 10 μm. Since this is small relative the spatial scale of compression, the formation of a reasonably well defined contact surface can be expected. The stability of this contact surface during the implosion, however, is a separate matter which is much more complex an issue and should be addressed in a future study of the concept.

In order for the magnetic flux to be trapped within the target plasma during the implosion, the plasma conductivity must be sufficiently high so that magnetic diffusion across the contact surface is sufficiently slow compared to the velocity of implosion. The ratio of the rate of implosion to the rate of magnetic diffusion is given by the magnetic Reynolds number of the process,

$$R_m = \mu\sigma v l$$

where μ, σ, and l are the permeability, conductivity and the spatial scale of the implosion. Using a temperature of about 100 eV and a velocity of 100 km/s for the contact surface, and setting l to be about half of the target radius, the Reynolds number is conservatively estimated to be at least 500. This is sufficiently large to ensure that magnetic flux leakage from the target plasma is negligible during the implosion.

4. Implosion Dynamics: Physical Description

The parameter space relevant to MTF has been extensively studied by Lindemuth and Kirkpatrick[13], and Kirkpatrick, Lindemuth and Ward[14]. Presenting the results in a plane with the

---

[12] R. A. Gross, *Fusion Energy*, John Wiley, New York, (1984).

[13] I. R. Lindemuth, and R. C. Kirkpatrick, "Parameter Space for Magnetized Fuel Targets in Inertia Confinement Fusion," Nucl. Fusion, **23**, p. 263, (1983).

[14] R. C. Kirkpatrick, I. R. Lindemuth, and M. S. Ward, "An Overview of Magnetized Target Fusion,," Fusion Technology, **27**, p. 201 (1995).

ion temperature and areal density (density-radius product) as coordinates (a Lindl-Widner diagram), the emphasis of these studies is in identifying the region of the parameter space in which fusion ignition would occur in the target, i.e. the condition of a positive rate of temperature rise ($dT/dt > 0$) in the target is maintained by the fusion reactions occurring in the target alone without further external energy input. Though target ignition is not a strict requirement for a workable scheme here, it is desirable. Our first objective in the following discussion is to explore the existence of practical target implosion trajectories leading to ignition.

There is, however, another important energetic consideration here, namely, the energy of the liner required to achieve the target ignition conditions. This issue has been examined for solid liners[15] where it is found that typically less than one-fifth of the initial liner energy is transferred to the target. We could expect a lesser proportion of the energy going into the target in the case of a plasma liner as more energy would be expended as thermal energy in the plasma liner during the implosion. On the other hand, the target gain has the potential of being amplified many times by the fusion burning of a thin but dense inner layer of the plasma liner. Our second objective in the following discussion is to provide estimates of the liner energy required to achieve the desired implosion, and to provide some indications of the possibility of the fusion burning of a thin inner layer of the liner.

A definitive study of these issues requires an accurate accounting of the energy deposition by the fusion α particles in a strong magnetic field. While efforts are underway to develop more accurate theoretical approaches and the computing methods to treat α-transport in a strong magnetic field, for convenience, we will adopt here an approximate model of Kirkpatrick in which an uniform azimuthal magnetic field is assumed to exist within the spherical volume of the target plasma.

To begin the discussion, assume a plasma liner in the form of a spherical shell of finite thickness converging on a target plasma which is also assumed to be spherical. As the plasma liner and the target plasma are initially relatively cold with relatively low sound speed, when they collide, shock waves are produced in both the target plasma and the liner. The shock in the target plasma converges spherically towards the center and is reflected near the center. In time, the reflected shock meets the radially converging contact surface giving rise to a second radially ingoing shock in the target which is again reflected near the center. The process is repeated until the radial momentum of the liner is totally dissipated, at which point the target and the liner have reached their peak compression. By design, the first ingoing and reflected shocks in the target are strong. The passage of these two shocks, however, heats the target to a sufficiently high temperature that the subsequent reflected shocks are relatively weak. The associated compression of the target plasma resulting from these weak shocks is more or less acoustic. If the magnetic field in the plasma is sufficiently high to provide the required degree of magnetothermal insulation, then the subsequent acoustic compression is nearly adiabatic.

The stability of this acoustic implosion phase is critical to the success of the scheme, and is determined by the Rayleigh-Taylor instability. In this study, we assume that the Rayleigh-Taylor instability becomes significant only for implosion with radial convergence of more than a factor

[15] S. A. Colgate, A. G. Petschek, and R. C. Kirkpatrick, "Minimum Energy for Fusion Ignition, A Realistic Goal," Los Alamos National Laboratory Report LA-UR-92-2599 (1992).

of 10. Accordingly we limit the radial convergence during the acoustic implosion to be less than 10. It must be appreciated that the driver of Rayleigh-Taylor instabilities during the implosion is the significant deceleration of the liner due to the pressure build-up in the target and the adverse density gradient across the target-liner interface. During the merging and coasting of the liner towards the target prior to impact, both the deceleration and density gradient are not sufficiently adverse to produce any significant growth rate for the Rayleigh-Taylor instabilities in the liner. Thus the radial convergence of the liner itself prior to its interaction with the target is not significantly subjected to this mode of instability.

After peak compression is reached, further advance by the liner is halted by the immense pressure developed in the target. A stagnating shock propagates outward in the liner with a "piston" speed approximately equal to the local inward flow speed before the arrival of the stagnating shock. When this stagnating shock reaches the outer boundary of the liner, a rarefaction wave propagates backwards towards the center. The confinement time for the target plasma is approximately the transit time of the stagnation shock plus twice the transit time of the rarefaction wave. During this period, the target plasma is designed to ignite or burn. Furthermore, the fusion α-particles leaving the target plasma still carry sufficient energy to cause an inner layer of the liner to burn (ignition is not required for the liner) to produce amplification of the energy gain of the target. The burn time for this inner "cold fuel layer" of the liner is approximately twice the transit time of the rarefaction wave.

5. Implosion Dynamics: The Mathematical Models

A succinct presentation of the mathematical models for analysing the concept is given here in support of the objectives of the present paper. Detailed discussion of the mathematical models are presented elsewhere.

5.1 The Preliminary Shock Heating and Compression of the Target Plasma

For the first ingoing shock, the Hugoniot jump conditions across the shock give the density (ρ_i), pressure (p_i), and temperature (T_i) behind the shock front in terms of the initial target density (ρ_0) and temperature (T_0) as,

$$\rho_i = \frac{\gamma+1}{\gamma-1}\rho_0, \qquad p_i = \frac{\gamma+1}{2}\rho_0 u_c^2, \qquad kT_i = \frac{\gamma-1}{1+Z_i}\frac{1}{2}m_i u_c^2. \tag{5.1}$$

assuming the shock to be infinitely strong (upstream Mach number $M \to \infty$) where m_i is the ion mass, u_c is the velocity of the contact surface, and Z_i is the effective charged state of the ions. The radially converging flow following the shock compresses the gas adiabatically by another factor of 4.719 for a gas with $\gamma = {}^5/_3$ according to Lazarus and Richtmyer[16]. The temperature rises by a factor of 2.813 associated with this adiabatic compression. The interaction of the ingoing flow with the stagnating flow near the center produces a reflected shock with a strength (pressure ratios) of 2.55. The corresponding upstream Mach number is 2.24, giving rise to a density

[16] R.B. Lazarus and R.D. Richtmyer, *Similarity Solutions for Converging Shocks*, Los Alamos Scientific Laboratory Report, LA-6823-MS, June 1977, Los Alamos, New Mexico, USA.

multiplication factor of 1.71 and a heating factor of 1.49667. The net density compression factor after the passage of the first ingoing and relected shock is thus 32, whereas the target plasma temperature is raised to the value T_{2s} given by,

$$kT_{2s} = \frac{2.797}{1+Z_i}\left(\frac{m_i u_c^2}{2}\right). \tag{5.2}$$

Denote the liner velocity before its collision with the target plasma by $u_{l,o}$. On impact with the target plasma, the liner sees a "piston" velocity of $u_{l,p} = u_{l,o} - u_c$ producing a shock propagating outwards relative to the liner. The resulting velocity of the contact surface u_c is one that results in a shock pressure in the liner that maintains pressure continuity across the contact surface. If the initial unshocked (upstream) pressure in the liner is $p_{l,o}$, applying the shock Hugoniot across the shock front in the liner gives the relationship,

$$\frac{1}{2}\rho_{l,0}u_{l,p}^2\left[(\gamma+1)p_i + (\gamma-1)p_{l,0}\right] = \left[p_i - p_{l,0}\right]^2 \tag{5.3}$$

Together with the expression (5.1) for the interfacial shocked pressure p_i, the two equations may be solved for the initial velocity of the contact surface u_c and the pressure p_i. In dimensionless form, the two equations may be reduced to one in terms of the upstream Mach number, $M_{l,s}$, of the shock front in the liner:

$$\begin{aligned} &\frac{1}{2}\gamma(\gamma-1)M_{l,s}^2\left(\frac{\gamma+1}{\gamma-1}\right)\left[\delta\left(M_l - M_{l,s}\right)^2 + 1\right] = \left[\delta\left(M_l - M_{l,s}\right)^2 - 1\right]^2 \\ &M_{l,s} = \frac{u_{l,p}}{c_{l,0}}, \quad M_l = \frac{u_{l,0}}{c_{l,0}}, \quad \delta = \frac{\gamma(\gamma+1)}{2}\left(\frac{\rho_0}{\rho_{l,0}}\right) \end{aligned} \tag{5.4}$$

where $c_{l,0}$ is the acoustic speed in the liner before colliding with the target plasma. We note that, in equation (5.4), $M_{l,s} = 0$ when the right hand side $\delta\left(M_l - M_{l,s}\right)^2 - 1 = 0$, or equivalently, when $\delta = 1/M_l^2$. This is the case when the impact is perfectly matched "acoustically" for the liner, resulting in no shock ($M_{l,s} = 0$) in the liner. For the case γ= 5/3, this condition reduces to requiring the liner velocity to be given by $u_l = \sqrt{(9/20)(\rho_{l,0}/\rho_0)}\,c_{l,0}$. The resulting instantaneous velocity of the contact surface equals this velocity. Equivalently, the resulting instantaneous shocked pressure in the target plasma at the interface is equal to the liner pressure ($p_{l,0}$) prior to impact. The liner velocity and pressure refers to these quantities at the inner surface of the liner.

5.2 The Accoustic Implosion Phase With Magnetic Thermal Insulation

The D-T reaction is selected for this first study, though the mathematical model developed may be extended to apply to other fusion reactions. The evolution of the target plasma temperature is governed by the energy equation,

$$\frac{d}{dt}(kT_t) = \frac{1}{6N}\left\{\Delta E_\alpha \dot{N}_r - \dot{Q}_c - \dot{Q}_{rad} - p\dot{V} - \dot{E}_B - \dot{E}_k\right\} \tag{5.5}$$

where N is the number of deuterons in the target plasma, ΔE_α is the amount of energy deposited by an α-particle in the target, $\dot{N}_r$ is the rate of fusion reactions, $\dot{Q}_c$ is the thermal conduction loss rate, $\dot{Q}_{rad}$ is the radiative loss rate, p is the target plasma pressure and $\dot{V}$ is the rate of change of the target volume, $\dot{E}_B$ is the rate of increase of the target magnetic energy, and $\dot{E}_k$ is the rate of change in the target kinetic energy. An equal mixture of D and T is assumed. The expressions for these quantities are given respectively by,

$$\dot{N} = -\dot{N}_r = -\frac{N^2}{V}\langle\sigma v\rangle,$$

$$\dot{Q}_c = 4\pi r_b^2 g\kappa\frac{T_t - T_b}{r_b}, \quad \kappa = \kappa_{\perp e} + \kappa_{\perp i}, \quad \kappa_{\perp e} = \frac{n_e k(kT_e)\tau_{ee}}{m_e}\frac{4.66\omega_{ce}^2\tau_{ee}^2 + 11.92}{\omega_{ce}^4\tau_{ee}^4 + 14.79\omega_{ce}^2\tau_{ee}^2 + 3.77},$$

$$\kappa_{\perp i} = \frac{n_i k(kT_i)\tau_{ii}}{m_i}\frac{2\omega_{ci}^2\tau_{ii}^2 + 2.64}{\omega_{ci}^4\tau_{ii}^4 + 2.7\omega_{ci}^2\tau_{ii}^2 + 0.68}, \quad \tau = \frac{25\pi m^{1/2}\varepsilon_0^2(kT)^{3/2}}{\sqrt{3}Z^4 ne^4\ln\Lambda}, \quad \omega_c = \frac{eB}{m}$$

$$\dot{Q}_{rad} = \dot{Q}_{bremsstrahlung} + \dot{Q}_{synchrotron},$$

$$\frac{\dot{Q}_{bremsstrahlung}}{V} = 1.445\times10^{-40} g_{ff} n_e T_e^{1/2} \qquad n_i Z_i^2, \quad \frac{\dot{Q}_{synchrotron}}{V} = 6.2\times10^{-17} B^2 n_e T_e(keV)\left(1 + \frac{T_e(keV)}{204} + \ldots\right),$$

$$\dot{E}_B = \frac{2\pi}{3\mu}\left(\frac{r_0}{r_h}\right)^2 (B_0 r_0)^2 u_b, \quad E_k = \frac{3}{10} m_t u_b^2, \quad p\dot{V} = \frac{3N_p kT_t u_b}{r_b}, \quad N_p = 4N. \tag{5.6a}$$

where r_b is the target plasma radius, V is its volume, u_b is its surface radial velocity, m_t is its mass, and T_b is the temperature of the "cold" boundary in contact with the liner (about 100 eV). N_p is the total number of particles (deuterons, tritons, and electrons) in the target plasma, and we have assumed that any fusion α-particles are instantaneously lost from the target after depositing a certain amount of energy ΔE_α in the target. SI units are used in the expressions throughout this Section, including the expressions that follow, except in the expression for synchrotron radiation above where the electron temperature is given in keV. The parameter g in the thermal conduction loss rate is a shape factor for the temperature profile within the target. For a parabolic temperature profile, g = 1.25. The thermal conductivities, $\kappa_{\perp e}$ and $\kappa_{\perp i}$, are Braginskii conductivities in the form given by Sheehey[17]. For the electron-electron (τ_{ee}) and ion-ion (τ_{ii}) collision times, we adopt the form for the collision time (τ) between like species given by Gross[18]. For α energy deposition ΔE_α in the presence of a magnetic field, Kirkpatrick[19] provides the following expression for the fractional α-deposition,

---

[17] P. T. Sheehey, *Magnetohydrodynamic Simulation of Solid-Deuterium-Initiated Z-Pinch Experiments*, Los Alamos National Laboratory Report LA-12724-T, p. 39, (3.1.7), (3.1.8), Los Alamos, New Mexico, USA, 1994.
[18] R. A. Gross, *Fusion Energy*, p. 53, (4.18), John Wiley, 1984.

$$f_\alpha(Br, \rho r; f_0) = f_0(\rho r)\,\frac{1+3(Br)^2}{1+3(Br)^2 f_0(\rho r)}\,, \qquad (5.6b)$$

where B is the constant azimuthal magnetic field, r is the radius of the plasma sphere, ρ is its mass density, and $f_0(\rho r)$ is the fractional α-deposition in the absence of the magnetic field. Expression (5.6b) was obtained by Kirkpatrick by fitting the analytical expression to the numerical results from an extensive run of a particle-tracking code. For α-deposition in the absence of the magnetic field, we use Evans' theory[20] in which the average spatial loss rate in energy by an ion of energy E, mass m and charge Ze to a particle species j in a plasma at a temperature T_j, mass m_j and charge $Z_j e$, is found to be,

$$-\left\langle \frac{dE}{dx} \right\rangle_j = 2\pi Z^2 Z_j^2 \left(\frac{e^2}{4\pi\varepsilon_0}\right)^2 \frac{m}{m_j E} F_j(y_j) \ln\Lambda_j\,,$$

$$F_j(y_j) = erf(y_j) - \left(1+\frac{m_j}{m}\right) y_j \frac{2}{\sqrt{\pi}} \exp(-y_j^2) \quad y_j^2 = \frac{m_j}{m}\frac{E}{kT_j}. \qquad (5.6c)$$

The loss rates to the ions and electrons are computed - separately and then summed.

5.3 The Structure of the Plasma Liner

Assuming the jets merge to form a steady-state gas shell with radial flow prior to impact, the flow velocity and density profiles may be computed by solving the steady-state fluid equations for mass and momentum conservation,

$$\frac{f}{fr} r^2 \rho u_r = 0, \quad \frac{fp}{fr} + \frac{1}{r^2}\frac{f}{fr}\rho r^2 u_r^2 = 0\,. \quad (5.7)$$

Furthermore, if we assume that the flow is polytropic with a polytropic index of Γ, these equations can be reduced to a single ordinary differential equation for the velocity profile, $\psi(\xi)$, in dimensionless form,

Figure 5.1. Liner profile

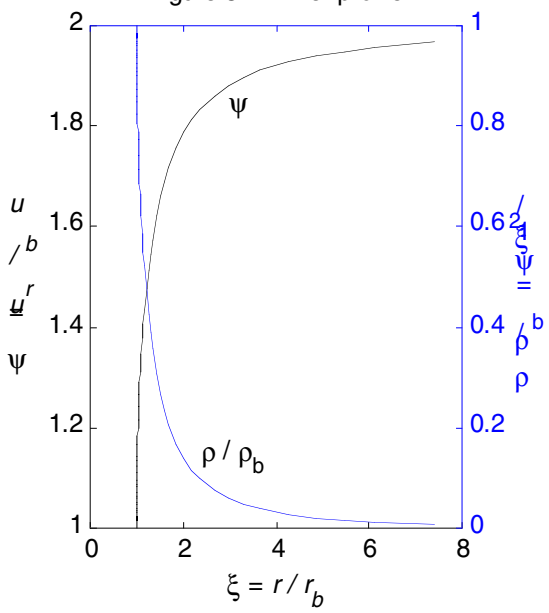

$$\frac{\xi}{2\psi}\frac{d\psi}{d\xi} = \frac{1}{M^2-1}, \quad M^2 = \left(\frac{u_r}{c}\right)^2 = M_b^2 \psi^{\Gamma+1}\xi^{2(\Gamma-1)}, \quad \psi = \frac{u_r}{u_b}, \quad \xi = \frac{r}{r_b}, \quad \psi(1) = 1, \quad (5.8)$$

---

[19] R.C.Kirkpatrick, private communication, November, 1998.

[20] F. Evans, *Note on the Calculation of Energy Deposition of Alpha Particles in a DT Plasma by Rutherford Scattering*, Los Alamos National Laboratory Report LA-5448-MS, 1973.

where c (= $\gamma p/\rho$) is the local sound speed at the position r, u_b, r_b, and M_b are the velocity, radial coordiate and the local Mach number of the inner surface of the liner respectively. The pressure, density and local sound speed at a point interior to the liner are given respectively by,

$$\frac{\rho}{\rho_b} = \left(\psi\xi^2\right)^{-1}, \qquad \frac{p}{p_b} = \left(\frac{\rho}{\rho_b}\right)^{\Gamma}, \qquad \frac{c}{c_b} = \left(\frac{\rho}{\rho_b}\right)^{(\Gamma-1)/2}, \tag{5.9}$$

where the subscript b refers to the inner surface of the liner. The velocity and density profiles obtained by a numerical solution of equation (5.8) for the case $M_b = 1^+$ are shown in Figure 5.1. Note the very steep gradient of both the density and the velocity profile near the interface. Note also that the knee of the velocity profile occurs around $\xi \sim 4$ and asypmtotes to a value twice its value at the interface. For $M^2 >> 1$, the equation has the asymptotic solution,

$$\psi \blacklozenge \quad 1 + \frac{1}{M_b^2}\left(\frac{\Gamma+1}{\Gamma-1}\right)\left(1 - \frac{1}{\xi^{2(\Gamma-1)}}\right)^{1/(\Gamma+1)}. \tag{5.10}$$

If the flow within the liner is adiabatic, then the polytropic index coincides with the ratio γ for the specific heats of the gas.

The total mass, thermal energy and kinetic energy of the liner are given respectively by,

$$\begin{aligned} m_l &= \int_V \rho \, dV = 3\rho_b V_b \int_1^{\xi_a} \frac{1}{\psi} \, d\xi, \\ E_{l,T} &= \int_V \frac{p}{\gamma-1} \, dV = \frac{3p_b V_b}{\gamma-1} \int_1^{\xi_a} \frac{\xi^2}{\left(\psi\xi^2\right)^{\gamma}} d\xi, \quad E_{l,k} = \int_V \frac{1}{2}\rho u_r^2 \, dV = \frac{3\gamma}{2} M_b^2 \int_1^{\xi_a} \psi \, d\xi. \end{aligned} \tag{5.11}$$

5.4 Target Confinement

The flow in the liner starts out highly supersonic with the local mach number M_b at the inner surface of the liner exceeding the value of 10 typically. By design, the initial momentum density of the liner is chosen to be such that compression of the target proceeds with very little resistance until near the point of turn-around. Near the point of turn-around, the sudden build up of pressure in the target and in the liner causes the flow in the liner to experience a rapid transition to a subsonic flow. A singularity is apparent in equation (5.8) at M = 1. Before the subsonic transition, equation (5.8) gives a reasonable approximation to the flow. It is used to compute the liner profile (velocity $u_r(r)$, density ρ(r), and pressure $p(r)$) down to the point when the local mach number M_b at the inner liner surface is nearly 1. At this point maximum compression in the target and liner is essentially attained, and a stagnation shock propagates outwards halting the converging flow in the liner. The "piston" speed of this stagnation shock is the local flow speed u_r. Thus, assuming that it is a strong shock, the local speed of the stagnation shock front is $(\gamma+1)u_r/2$. The transit time for this stagnation shock is approximated by the integral,

$$t_s = \frac{2}{\gamma+1}\int_{r_b}^{r_a}\frac{dr}{u_r} = \frac{r_b}{u_b}\sqrt{\frac{2}{\gamma+1}}\int_1^{\xi_a}\frac{d\xi}{\psi(\xi)} \ldots \frac{r_b}{u_b}\tau_s(\xi_a). \tag{5.12}$$

where the dimensionless velocity profile $\psi(\xi)$ is calculated from equation (5.8) with $M_b = 1^+$, as shown in Figure 5.1.

When the stagnation shock reaches the outer boundary of the liner ($r = r_a$), a rarefaction wave propagates backwards. The rarefaction wave speed is approximately the local speed of sound. Hence an estimate of its transit time may be given by,

$$t_r = \frac{dr_s}{c_s(r_s)},$$

where $c_s(r_s)$ is the local sound speed at the shocked radial position r_s. After the passage of the stagnation shock, the shocked density $\rho_s(r_s)$ and the shocked pressure $p_s(r_s)$ at the shocked position r_s, are given respectively by,

$$\rho_s(r_s) = \frac{\gamma+1}{\gamma-1}\rho(r), \quad p_s(r_s) = \frac{\gamma+1}{2}\rho(r)u_r^2(r), \tag{5.13}$$

where ρ(r) and $u_r(r)$ are the density and velocity at the unshocked position r before the passage of the stagnation shock. The shocked (r_s) and unshocked (r) coordinates are related by mass conservation as,

$$4\pi r^2\rho(r)\,dr = 4\pi r_s^2\rho_s(r_s)\,dr_s, \quad \text{or,} \quad dr_s = \frac{\gamma-1}{\gamma+1}\int^{1/3}\frac{\xi^2}{\xi^3 + \frac{2}{\gamma-1}}^{2/3}\,dr. \tag{5.14}$$

The rarefaction wave transit time integral is accordingly given by,

$$t_r = \frac{r_b}{u_b}\sqrt{\frac{\gamma-1}{\gamma+1}}\int^{1/3}\frac{2}{\gamma(\gamma-1)}\int_1^{1/2}\frac{\xi^2}{\xi^3 + \frac{2}{\gamma-1}\psi^{2/3}}\,d\xi \ldots . \frac{r_b}{u_b}\tau_r(\xi_a) \tag{5.15}$$

The target confinement time is taken to be,

$$t_{conf} = t_s + 2t_r = \frac{r_b}{u_b}(\tau_s(\xi_a) + 2\tau_r(\xi_a)). \tag{5.16}$$

5.5 Estimating the Yield from the Burning of the Cold Fuel Layer

Let $\varepsilon_s(r_s)$ be the energy density at the position r_s after the passage of the stagnation shock, but before the passage of the alpha particles streaming outwards from the fusion burning target. After the passage of the alpha particles, the energy density at the point is increased by the energy deposition by the target alpha particles. The resulting energy density and temperature at the position r_s in the liner are,

$$\varepsilon = \varepsilon_s + \left(-\frac{dE_\alpha'}{dr}\right)\left(\frac{N_\alpha}{4\pi r_s^2}\right) = \frac{1}{2}\rho_s(r_s)u_r^2 + \left(-\frac{dE_\alpha'}{dr}\right)\left(\frac{N_\alpha}{4\pi r_s^2}\right) = \frac{1}{2}\rho_b u_b^2\left(\frac{\gamma+1}{\gamma-1}\right)\left(\frac{\psi}{\xi^2}\right) + \left(-\frac{dE_\alpha'}{dr}\right)\left(\frac{N_\alpha}{4\pi r_s^2}\right),$$

$$kT = \frac{(\gamma-1)\varepsilon}{2n_{DT}}, \tag{5.16}$$

where $n_{DT} = \dfrac{\rho_s(r_s)}{m_{DT}}$, and N_α is the cumulative (total) number of alpha particles passing through the spherical shell at position r_s. The spatial rate of energy deposition by the alpha particles to the plasma, $-\dfrac{dE_\alpha'}{dr}$, is given by Evans' theory, expression (5.6c). This is calculated using the density and temperature profile of the liner before the passage of the alpha particles. The decrease in the energy of the alpha particle is accounted for by integrating Evans' equation (5.6c) over this profile for the passage of the alpha particles through the liner. Knowing the temperature T, the local fusion reactivity $\langle\sigma v\rangle$ and the fusion reaction rate can be determined. The burn fraction f_b at this position follows if the burn time is known.

We have not taken into account the increase in the temperature of the liner and the fusion reactivity due to the energy deposition of the new alpha particles born of the fusion in the liner. Thus yield enhancement of a propagating burn through the liner has not been included here. On the other hand, this increase in temperature and pressure would lead to a local expansion and a consequent reduction of fusion reactivity and its yield. Overall we expect that the results produced here are a conservative approximation and the overall fusion yield is likely to be larger than what we present here.

Most of the burn in the liner occurs in a very thin inner layer (of the order of several to a few tens of μm's) of the liner where the density is high. The burn time for this thin inner layer is taken to be twice the rarefaction wave transit time t_r as given by experession (5.15). The total fusion yield from the burning of the cold fuel layer is estimated by integrating the fusion energy density over the volume of the burning layer in the liner, thus,

$$E_{Fl} = N_r\varepsilon_F = \varepsilon_F \int 4\pi r_s^2 f_b n_D \, dr_s, \quad \varepsilon_F = 17.6 \text{ MeV for D - T reactions.} \tag{5.17}$$

5.6 Implementation

The mathematical models were implemented in a suite of MATLAB codes. Detailed documentation of the codes is given elsewhere[21]. The analysis begins by specifying the target radius, ion density, temperature and magnetic field at the moment of impact with the liner. The impact is assumed to be acoustically matched for the liner. The shock compression and heating are calculated according to the theory developed in section 5.1. The resulting target conditions are then used as the initial conditions for the set of ordinary differential equations (5.5) and (5.6) of section 5.2 governing the acoustic compression of the target.

The differential equations are integrated using a 4^{th}-order Runge-Kutta method. During the early stages of the acoustic compression, because of the overwhelming momentum density of the liner, the trajectory is more or less linear. In the calculation, a linear trajectory is assumed until desired peak compression is nearly reached. To provide a smooth transition to the state in which the liner is stationary, when the time is within 10% of the instant of peak compression, a quartic time dependence of the target radius is assumed until the target radius reaches a pre-assigned minimum value. After this instant, the target radius is kept constant computationally for a length of time which is the target and liner confinement time as defined in Section 5.4. Time integration of the differential equations is continued until a preset instant, giving the temperature, the cumulative number of fusion reactions, and the alpha energy deposition in the target versus time. The p-dV work done on the target is also accumulated versus time.

The peak pressure of the nuclear burning target and the confinement time together determines the pressure, density and the thickness of the stagnated liner, and hence the energy in the liner at stagnation. Adding to this the energy required to perform the p-dV work on the target, and the shock heating and compression due to the first ingoing and reflected shock, gives the minimum kinetic energy the liner must have initially. The maximum pressure experienced by the target up to a particular instant t determines the inner pressure p_b of the liner required to confine the target. Following Section 5.3 above, the profile of the liner at peak compression is taken to be its profile when the mach number M_b of the flow at the inner liner surface is $\sim 1^+$. By similarity of the flow, the flow velocity at the inner surface at impact is approximately the asymptotic value of its velocity profile at peak compression, assuming a compression ratio > 4. The flow velocity at the inner liner surface at peak compression is thus about half the contact surface velocity at impact ($u_b \sim 0.5\ u_c$). The inner liner density is determined from these data as $\rho_b = \gamma p_b / c_b^2$. With the value of u_b known, the required confinement time determines the dimensionless position ξ_a of the outer boundary of the liner through the relationship (5.15). The integrals (5.11) then give the mass and energy of the liner at this position required to confine the target in pressure and time. The fusion yield of the liner follows from the expressions (5.16) and (5.17) of Section 5.5 given the fusion yield from the target and the liner profile.

Finally, the structure of the liner prior to impact is calculated by requiring mass and energy conservation. Thermal losses from the liner are ignored (liner performance is expected to improve if thermal losses from the liner are taken into account as they would produce a colder

[21] Y.C.F. Thio, *Computer Codes for Modeling the Implosion of a Magnetized Target Plasma by a Spherical Plasma Liner*, Center for Space Plasma and Aeronomic Research Report, University of Alabama, Huntsville, Alabama, December, 1998.

and denser liner). The energy of the liner prior to impact is the sum of the energy required to produce the first ingoing and reflected shocks in the target, the p-dV work on the target during the acoustic compression of the target, and the energy of the liner at peak compression.

6. Implosion Dynamics: The Numerical Results and Discussion

Computations are conducted here only to show the existence of realizable implosion trajectories to produce substantial fusion yield and meaningful gain, and to illustrate the profound effect the magnetic field has on the outcomes. Extensive parametric studies are left for the future. A small number of cases are computed here for an almost arbitrarily chosen implosion velocity of 125 km/s. The radius and the DT ion density of the target at impact with the liner are chosen to be 50 mm and 10^{24} m^{-3} respectively. After the first ingoing and reflected shocks, the target shrinks to a radius of 15.8 mm and a shock heated temperature of about 283 eV, quite independently of its initial temperature. The computation proceeds to model the thermal evolution of the target plasma as it is acoustically compressed down to a preset radius of 2.5 mm. The acoustic radius compression ratio is 6.3. The target is then computationally maintained at the minimum radius for a length of time which is the confinement time of the target as defined in Section 5.4. The thermal evolution of the target and the consequent fusion yield from the target and the liner is critically affected by the presence of the magnetic field and is illustrated here for four cases of the initial magnetic field in the target at impact. The computation then proceeds to determine the total liner energy required to confine the target as a function of the confinement time. For the same peak target pressure, the longer the confinement time required, the thicker is the liner and thus the larger is its thermal energy at stagnation. The principal computational results are summarized in Table 6.1.

Case #	#1	#2	#3	#4
Target B field at impact (T)	2	1	0.5	0
Target B field after the first two shocks	20.2	10.1	5	0
Radial convergence factor due to acoustic compression	6.3	6.3	6.3	6.3
Maximum target temperature (keV)	>36	9.96	8.3	1.5
Confinement time allowed (μs)	0-0.2	0-0.2	0-0.20	0-0.2
Target fusion yield (MJ)	0-216	0-52	0-9.1	0.0023
Liner fusion yield (MJ)	0-1220	0-1150	0-646	0
Liner energy (MJ)	0-94	0-38	0-32	4.4
Maximum system (target + liner) net gain	56	70	28	0.0017
Confinement time at max. gain (μs)	0.029	0.057	0.085	0.0078
Liner energy at max. gain (MJ)	11	13.7	15.7	1.1
Fusion yield at max. gain (MJ)	619	962	433	0.0019
Minimum liner thickness at max. gain (mm)	1.6	3.1	4.5	0.42
Ion density at the inner liner surface at peak compression at max. gain (m^{-3})	3.7×10^{30}	2.6×10^{30}	2.2×10^{30}	4×10^{29}
Target system gain (target yield/total input)	1.4	1.3	0.54	0.002

Table 6.1. Summary of cases computed and discussed.

A typical set of the modeling results are shown in Figures 6.1 (a) – (f), in which the case for an initial magnetic field B of 2 T in the target is illustrated. The target temperature (labeled T), the burn fraction of the target (labeled f_b) and the mean fractional alpha deposition in the target (labeled f_α) versus time measured from the end of the first ingoing and reflected shocks are shown in Figure 6.1(a). The temperature rises sharply when the target radius falls below 3 mm. When the compression stops, the target temperature is 12 keV. However, the target temperature continues to increase after the compression stops, climbing to about 36 keV after a target confinement time of 200 ns. Ignition occurs because of the high magnetic field of 800 T present in the target at peak compression. The high magnetic field gives rise to a high degree of α-deposition, reaching almost 40% just after peak compression is reached when the density is high and the temperature is not so high. The target burns rapidly generating a yield of nearly 216 MJ after having been confined for 200 ns, as shown in Figure 6.1(b). The same figure shows also that the total amount of energy invested in the target is 2.8 MJ. Defining self gain of the target as the ratio of target fusion yield to the energy invested in the target, the self gain of the target in this case is around 80.

The fusion yield from the target is amplified by the burning of a thin but very dense layer in the inner surface of the liner. The ion density in the inner surface of the liner reaches over 3.7×10^{30} m^{-3} at peak compression in this case as shown in Figure 6.1(f). At this density, the α-energy is rapidly absorbed in an extremely thin layer of the liner. The DT in this thin layer burns rapidly releasing nearly 1.2 GJ of fusion energy in less than 200 ns as illustrated in Figure 6.1(d). However, in order to provide a confinement time of 200 ns, the total energy required by the liner is 94 MJ. Defining the net gain Q_{net} to be the ratio of the total fusion yield to the total liner energy required, this gives a net gain of only 15 if a liner is used to provide a confinement time of 200 ns.

We note, however, that in this case, a confinement time of 200 ns is excessive and is not optimum with respect to net gain of the system. This is illustrated in Figure 6.1(c) in which the net gain is shown as a function of confinement time. The net gain peaks at a value of 56 for a confinement time of about 29 ns. The liner that provides this confinement time requires only 11 MJ of energy. The total fusion yield in this case is 619 MJ. The liner amplification, defined as the ratio of the liner yield to the target yield, is shown in Figure 6.1(d) as the curve labeled A. It peaks at a value of about 39 for about the same confinement time also. The burning of the liner occurs only in an extremely thin inner layer of the liner in which the α-particles originating from the target are totally absorbed because of the high density and the low temperature in the layer. Since burn propagation is not provided for in the present model, the fuel in this layer becomes depleted with increasing degree of burn. Therefore, the yield from this liner layer gradually plateaus (Figure 6.1(d)) while the required liner energy increases almost linearly with confinement time. This leads to a decline in liner amplification and net gain with confinement time after a peak is reached.

Finally, the liner thickness and density at various radial position as a function of confinement time are shown in Figure 6.1(e) and (f) respectively. The mathematical model as developed in Section 5.3 assumes that the flow profile in the liner is self similar with respect to its radial position. Thus its thickness scales linearly and its density inversely with the cube of its radial position. If the liner is formed at 0.25 m away from center, then its thickness and density at

formation are shown by the curves labeled *f* in Figure 6.1(e) and (f) respectively. Though the density of the compressed liner is high, its density at formation by the merging of the plasma jets, is relatively low, of the order of 2.4×10^{24} m^{-3}. The velocity of the liner at this position is about 128 km/s. These numbers of are indicative of the properties of the plasma jets required to form the liner.

In Figure 6.2 (a) – (d), the performance of the system is studied as a function of the initial target *B* field, as well as the target confinement time. Four values of the initial *B* field ($B(0)$) are used: 2, 1, 0.5 and 0 T, with the case of 2 T treated in Figure 6.1 included as a reference. The thermal evolutions of the target for the various initial B fields are shown in Figure 6.2(a), the net gains in Figure 6.2(b), the required liner energies in Figure 6.2(c), and the total fusion yield in Figure 6.2(d).

As expected, in the case $B(0) = 0$, there is no magnetothermal insulation and the target hardly gets above 1.5 keV in temperature. No meaningful fusion yield occurs in this case.

In the cases where $B(0) = 0.5$, 1, and 2 T, the effects of magnetothermal insulation are clearly in evidence. The temperature development follows similar trajectories for the three cases up to the point when the compression stops. At this point, the target with a $B(0) = 0.5$ T cools rapidly, indicative of the high rate of the thermal losses despite the presence of relatively strong magnetic field (200 T). Although the target temperature reaches 8.3 keV, the fusion rate and the α-deposition rate were not sufficiently high to maintain the temperature and the burning of the target. No target ignition occurs in this case. However, we note that the system consisting of the target and the liner together still gives rise to a significant net gain which peaks at about 28 for 85 ns of confinement, giving a total fusion yield of 433 MJ and requiring only about 16 MJ of liner energy. For the case with the highest $B(0)$ of 2T, the target temperature continues to rise because, with the target magnetic field at 800 T at peak compression, the α-deposition rate and the magnetothermal insulation are sufficiently high to produce ignition in the target. The net gain peaks in this case at 56 after 29 ns of target confinement, yielding 619 MJ of fusion energy with 11 MJ of energy input into the liner.

The real surprise is the existence of an intermediate value between 0.5 and 2 T, namely the case with $B(0) = 1$ T, where the net gain of the system actually rises above that of the case with $B(0) = 2$ T. A net gain of 70 was attained in this case after a target confinement time of 57 ns, yielding 962 MJ of fusion energy for only 13.7 MJ of energy input. The reason for this is that, while the fusion and α-deposition rate was such that the burning occurs below but at the verge of ignition, the fractional α-deposition rate in the target was lower than the case for $B(0) = 2$ T, allowing therefore a higher α energy flux into the liner. This gives rise to a higher heating rate of the inner layer of the liner. The necessary burn temperature in the liner for maximum fusion yield was reached in a shorter confinement time, requiring therefore less energy for the liner, resulting in a higher net gain. Notice that the total fusion yield plateaus in this case after the maximum gain was reached as illustrated in Figure 6.2 (d). This is evident of the 'burn-out' of the inner liner layer due to a combination high temperature and high density. In the present model, radiative and conductive thermal transport in the liner are neglected, so also the effect of local hydrodynamic expansion. These assumptions are likely to break down under these circumstances. Future studies should address these effects.

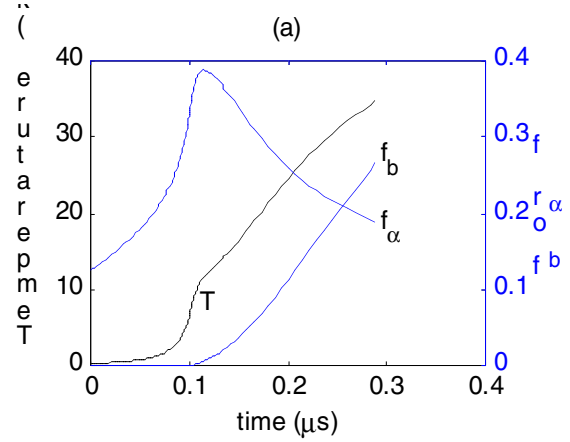

f_b - target burn fraction

f_α - fractional alpha deposition in target

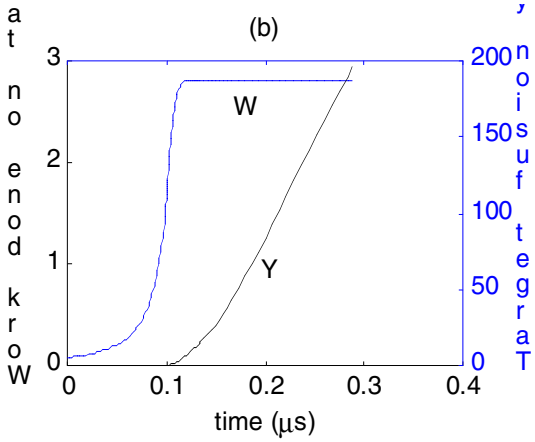

Y = Target yield

W = Work done on target

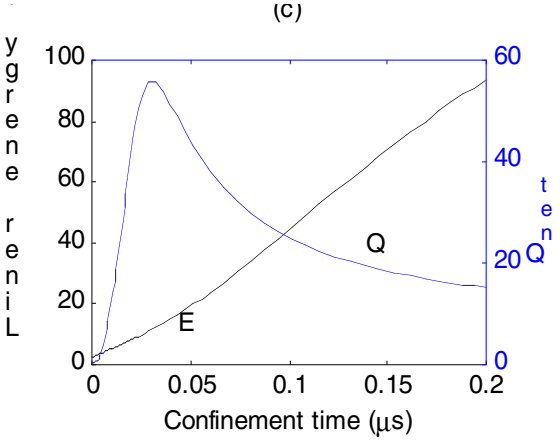

E - total liner energy

Q - net gain = total yield / input

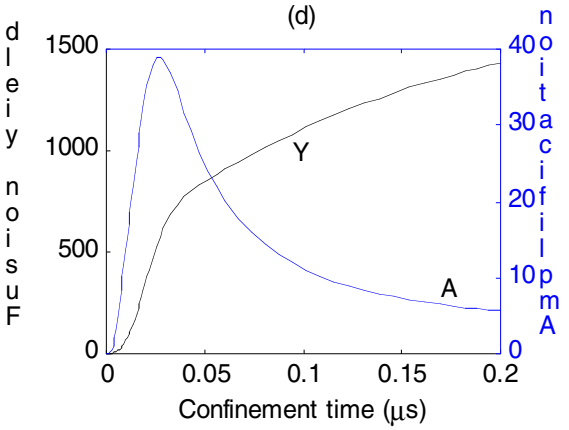

Y = Total yield (liner + target)

A = Liner yield / target yield

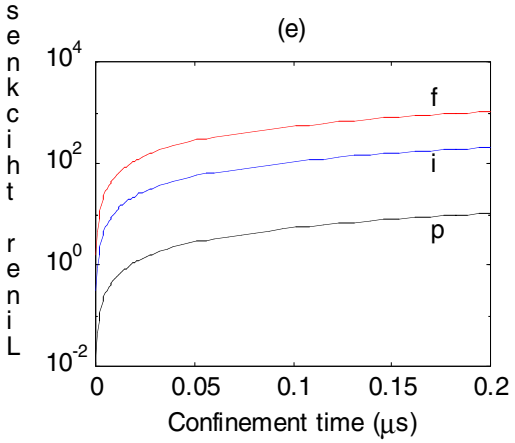

p - peak compression

i - at impact

f - at formation

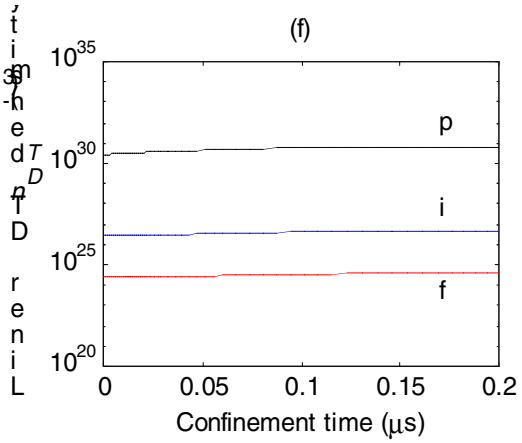

p - peak compression

i - at impact

f - at formation

Figure 6.1. Case A-1: B(0) = 2T, $n_i(0) = 1 \times 10^{24}$ m^{-3}, $v_b(0) = 125$ km/s, T(0) = 10 eV, r(0) = 50 mm, $r_p = 2.5$ mm.

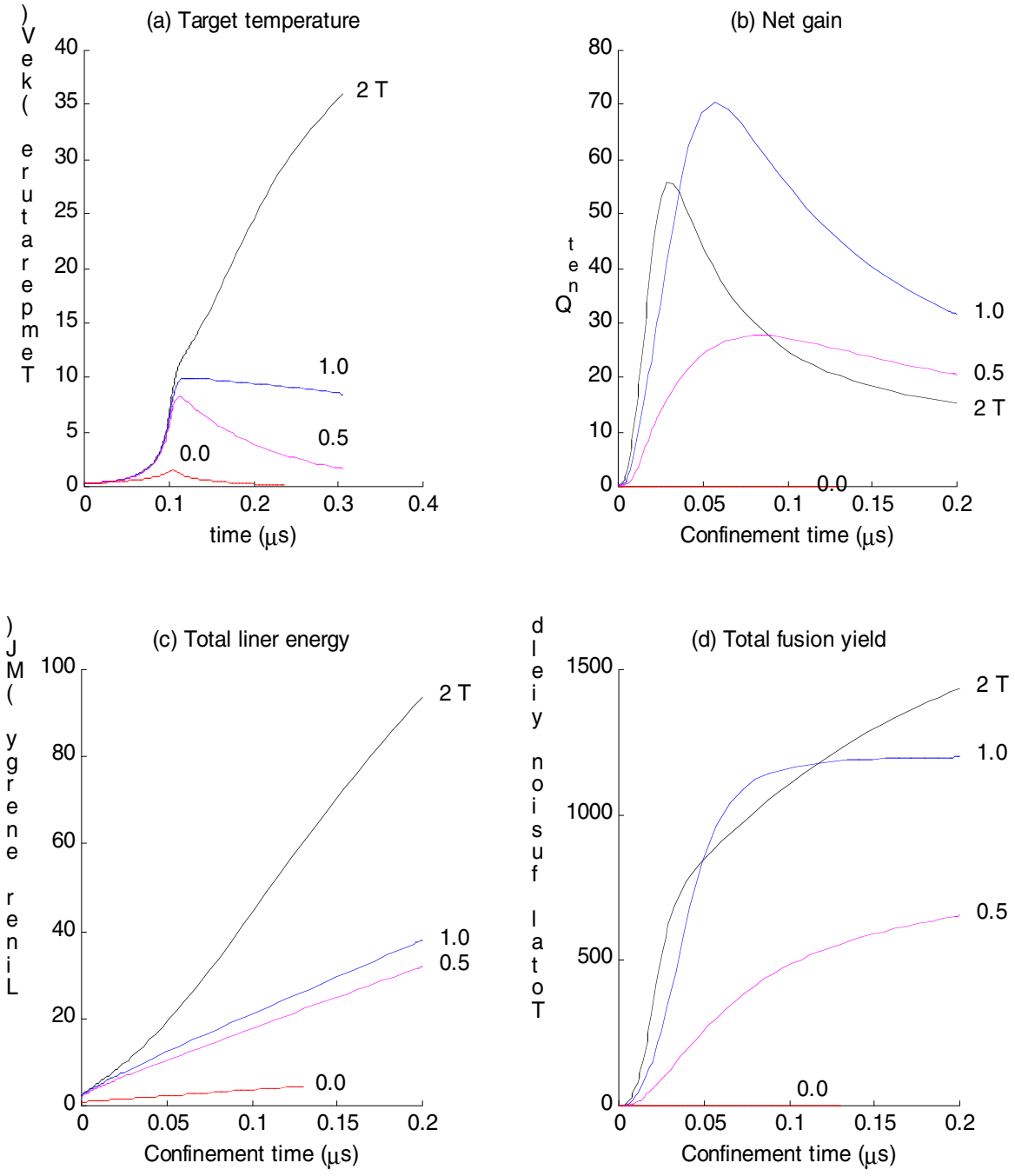

Figure 6.2. Performance as a function of the initial magnetic field in the target and confinement time. The different curves are for four different values of the initial target magnetic field: 0, 0.5, 1, and 2 T.

7.0 Conclusion

An embodiment of magnetized target fusion (MTF) with the potential that the drivers can be positioned in a standoff distance from the site of the fusion burn is proposed. The magnetized target plasma is formed out of two merging compact toroids, and is imploded by a spherical plasma liner formed out of the merging of a number (nominally 60) of high momentum density plasma jets. These plasma jets are produced by highly efficient electromagnetic accelerators, the efficiency of which is expected to exceed 50%. They also carry the main fusion fuel. The implosion dynamics is studied in three phases: the preliminary shock heating and compression, the acoustic compression, and the containment of the burning target and liner. Mathematical models are developed to model these three phases of the implosion dynamics, and have been implemented in a suite of computer codes. Preliminary results produced by the models have been very encouraging, showing the great potential of the proposed MTF scheme. The presence of the magnetic field in the target has profound effects on the implosion trajectories and the consequent fusion yield. The liner requirement to confine a specific target is a function of the confinement time and the initial magnetic field in the target, which together dictates the fusion yield from the target.

The model is applied to study the liner requirements to implode a specific target with an initial radius (50 mm), an initial DT density (10^{24} m^{-3}) to a final radius (2.5 mm) with an initial implosion velocity (125 km/s) at impact with the liner, versus the length of confinement time. Carrying out the computation for four discrete values of the initial target magnetic field (0, 0.5, 1 and 2 T), we found that: (1) The target temperature exceeds 8 keV in all cases except the case of no magnetic field, in which case, the temperature hardly exceeds 1.5 keV; (2) All cases produce substantial fusion yield with a significant system net gain except for the case with no initial magnetic field; (3) Substantial fusion yield with a significant system gain exceeding 28 can occur even without ignition in the target; (4) Ignition occurs for an initial magnetic field > 1 T; (5) For a particular value of the initial magnetic field, the system net gain increases at first with confinement time, reaches a peak and then declines with further increase in confinement time. (6) The maximum gain achieveable does not increase indefinitely with increasing initial magnetic field; rather, the maximum gain peaks at some value of the initial magnetic field; in the present case, it peaks near an initial magnetic field of 1 T; for this value, the maximum system gain occurs for a confinement time of 57 ns, with a total fusion yield of 962 MJ, requiring only 13.7 MJ of energy input into the liner and target, giving a net system gain of 70. Because electromagnetic accelerators are highly efficient, gains such as this or lower are more than adequate for a practical system for economical power generation. In this sense, these gains are relatively high for practical purposes. If the liner is formed at 25 cm from the center of implosion, the DT density of the liner is of the order of 1.6×10^{24} m^{-3}, which is indicative of the density of the plasma jets required.

The results show that further exploration of the concept are highly warranted. Parametric studies are needed to elucidate the scope of the practical potentials of the concept. The feasibility of merging the jets to form a spherical and/or cylindrical liner is a fundamental issue that warrants immediate attention theoretically and experimentally. The stability of the contact surface during the shock and acoustic compression phase should be investigated, so also are the effects of radiative and conductive thermal transfer on the structure of the liner. The potential enhancement

of the nuclear burn produced by a secondary implosion of the target caused by the burning of the inner layer of the liner should also be explored.

Acknowledgement

The development of the concept has benefited from the opportunities of presenting the concept at a number of meetings and conferences, including the IAEA TC Meeting in Pleasanton, California, October 20-23, 1997, the First International Workshop in MTF in the same place and time, the DoE Innovative Confinement Concepts Workshop at Princeton Plasma Physics Laboratory in April 1998, and the IEEE ICOPS at NCSU, Raleigh, North Carolina, June 1998. It has benefited greatly through the numerous discussions with a great number of people, among them, Richard Siemon, Irv Lindemuth, Pete Sheehey, Dan Barnes and Fred Ribe of Los Alamos National Laboratory, Jim Degnan and Gerry Kyuttu of the Air Force Research Laboratory at Kirtland AFB, Albuquerque, George Miley of the University of Illinois at Urbana-Champaign, Dimitri Ryutov and Ralph Moir of Lawrence Livermore National Laboratory, Nikos Salingarov of the University of Texas at St. Antonio, and others. We also like to thank Fleur Daniels (formerly) at Massey University, Auckland, New Zealand and Brent Freeze at the University of California at Los Angeles for assisting with the art work for Figures 2.1 and 2.2 respectively.